Proceedings of ERAD 2006

The impact of depolarization on polarimetric signatures in snow

Alexander Ryzhkov[1,2] and Dusan Zrnic[2]

[1]University of Oklahoma, Norman (USA).

[2]National Severe Storms Laboratory, Norman (USA).

1 Introduction

Simultaneous transmission and reception of Horizontally and Vertically polarized waves (SHV) is a preferable choice technique for dual-polarization weather radar (Doviak et al. 2000). One of the side effects of such a choice is possible cross-coupling between orthogonally polarized waves. Cross-coupling depends on depolarizing properties of propagation media and it is usually negligible in rain because the net mean canting angle of raindrops is close to zero (Doviak et al. 2000; Ryzhkov et al. 2002).

Snow crystals at the tops of thunderstorm clouds are often canted in the presence of strong electric fields and produce noticeable cross-coupling between radar signals at horizontal and vertical polarizations if both signals are transmitted and received simultaneously. As a result, unusually looking radial signatures of differential reflectivity Z_{DR} and differential phase Φ_{DP} are commonly observed in the crystal regions of thunderstorms.

The paper presents examples of strong depolarization in oriented crystals from the data collected by the polarimetric prototype of the WSR-88D radar and a theoretical model that explains the results of measurements.

2 Cross-coupling polarimetric signatures

Most frequently, cross-coupling polarimetric signatures are observed in deep convective and stratiform clouds associated with warm-season mesoscale convective systems (MCS). Two ingredients are necessary for the signature to exist: abundance of pristine, low-inertia crystals and sufficiently strong electrostatic field to orient such crystals.

A composite plot of radar reflectivity factor Z, differential reflectivity Z_{DR}, and differential phase Φ_{DP} at elevation 5.5° for the mesoscale convective system on June 21, 2004 is shown in Fig. 1.

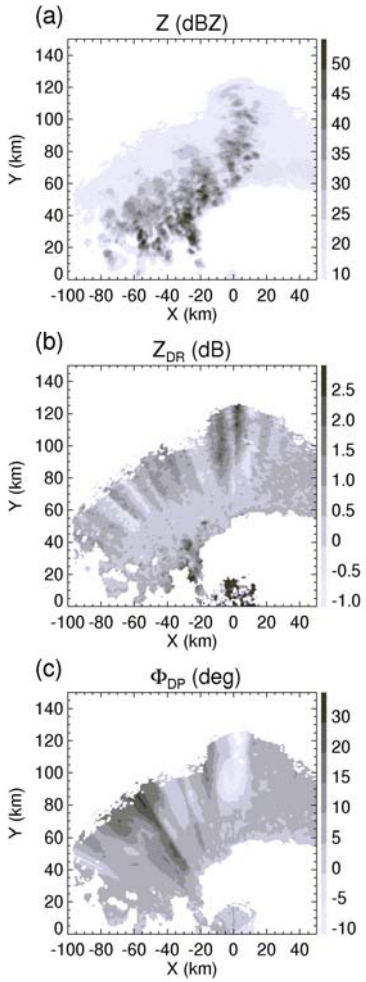

Fig 1. A composite plot of Z, Z_{DR}, and Φ_{DP} for the MCS observed with KOUN radar in Oklahoma on June 21, 2004; 0906 UTC, El = 5.5°. Simultaneous transmission / reception.

Numerous radial streaks of positive and negative Z_{DR} are evident in the crystal region of the cloud. These streaks are unlikely caused by differential attenuation in underlying liquid and mixed-phase hydrometeors because (a) Z_{DR} was corrected for differential attenuation and (b) if this were the case then the Z_{DR} radial features would be observed at closer slant ranges where dry aggregated snowflakes are dominant scatterers.

More detailed analysis of radial profiles of Z_{DR}, Φ_{DP}, and radar reflectivity factor at horizontal polarization Z indicates that the steepest slopes in the Z_{DR} range dependencies are associated with Z between 20 and 35 dBZ and with shallow local minima of Φ_{DP} (Fig. 2). Figure 2 exhibits strong azimuthal variability of the Z_{DR} range profiles within relatively narrow azimuthal sector.

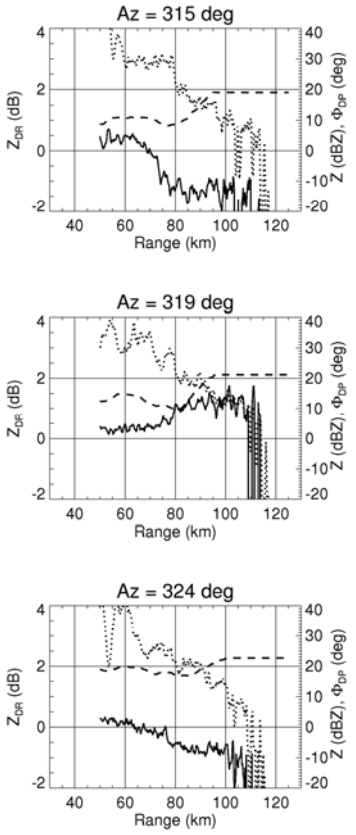

Fig 2. Radial dependencies of Z_{DR} (solid lines), Φ_{DP} (dashed lines), and Z (dotted lines) at three azimuthal directions and elevation 5.5° for the PPI presented in Fig. 1.

Most of radially elongated features in Z_{DR} originate at the tops of convective cells and the heights that usually exceed 7 - 8 km. Such a localization and obvious association with the areas of negative K_{DP} point to depolarization in canted crystals as a most likely cause of the signature. In the next section, we present relatively simple theoretical model which provides physical explanation of the Z_{DR} signatures and its relation to cross-coupling resulted from the use of the SHV scheme as opposed to more traditional alternate transmission and reception of orthogonally polarized waves.

3 Theoretical analysis. General formulas.

The voltage vectors of the transmitted ($\mathbf{V}^t$) and received ($\mathbf{V}$) waves are related as

$$\mathbf{V} = C\mathbf{S}'\mathbf{V}^t \quad , \qquad (1)$$

where

$$\mathbf{S}' = \widetilde{\mathbf{T}}\mathbf{S}\mathbf{T} \quad , \qquad (2)$$

$\mathbf{S}$ is the backscattering matrix representing properties of the scatterers in the radar resolution volume, $\mathbf{T}$ is a transmission matrix describing changes in the polarization state of EM wave as it propagates in the anisotropic medium, and C is a constant depending on the radar parameters and the distance between the radar and scatterers.

In the case of alternate transmission / reception $\mathbf{V}^t = (1,0)$ if H wave is transmitted and $\mathbf{V}^t = (0,1)$ if V wave is transmitted, whereas in the SHV mode $\mathbf{V}^t = (e^{-j\Phi_t},1)$, where Φ_t is a system differential phase upon transmission. In the alternate mode of operation

$$V_{h,v} = CS'_{hh,vv} \quad . \qquad (3)$$

If both H and V waves are transmitted simultaneously and H wave acquires additional differential phase Φ_r upon reception, then

$$V_h = Ce^{-j\Phi_r}(S'_{hh}e^{-j\Phi_t} + S'_{hv}) \qquad (4)$$

$$V_v = C(S'_{vv} + S'_{hv}e^{-j\Phi_t}) \qquad (5)$$

The terms proportional to S_{hv}' in (4) and (5) are caused by cross-coupling between H and V waves. These cross-coupling terms are not equal to zero if the mean canting angle of hydrometeors within the radar resolution volume is different from 0 or 90° or EM wave depolarizes as it propagates within anisotropic medium.

In our model, we assume that depolarization of EM waves occurs only in oriented crystals due to their nonzero mean canting angle and ignore much smaller depolarization in other hydrometeor types such as rain, graupel, hail, and wet / dry aggregated snow. Consequently, we divide the wave propagation path into depolarizing and nondepolarizing parts and express the transmission matrix $\mathbf{T}$ as a product of the matrix $\mathbf{T_{cr}}$ describing propagation in crystals and matrix $\mathbf{T_{nc}}$ which is attributed to the rest of the propagation path. As a result

$$\mathbf{S}' = \widetilde{\mathbf{T}}\mathbf{S}\mathbf{T} = \widetilde{\mathbf{T}}_{\mathbf{nc}}\widetilde{\mathbf{T}}_{\mathbf{cr}}\mathbf{S}\mathbf{T}_{\mathbf{cr}}\mathbf{T}_{\mathbf{nc}} = \widetilde{\mathbf{T}}_{\mathbf{nc}}\mathbf{S}''\mathbf{T}_{\mathbf{nc}} \quad , \qquad (8)$$

where

$$\mathbf{S''} = \widetilde{\mathbf{T}}_{\mathbf{cr}} \mathbf{S} \mathbf{T}_{\mathbf{cr}} \quad . \tag{9}$$

The matrix $\mathbf{T_{nc}}$ in nondepolarizing medium has a simple diagonal form with the elements

$$T_{hh,vv} = \exp(-j\Phi_{h,v} - \Gamma_{h,v}) \tag{10}$$

where $\Phi_{h,v}$ is phase shift and $\Gamma_{h,v}$ is attenuation referred to the nondepolarizing part of the propagation path. Differential phase Φ_{dp} is defined as

$$\Phi_{dp} = 2(\Phi_h - \Phi_v) \tag{11}$$

Throughout this paper, we distinguish between differential phase Φ_{dp} (lowercase subscript) associated with the nondepolarizing part of the propagation path and the measured total differential phase Φ_{DP} (uppercase subscript).

Substituting (8) - (11) into (4) and (5) yields

$$V_h = CT_{vv}^2 \xi e^{-j(\Phi_r + \Phi_{dp}/2)} (\xi e^{-j(\Phi_t + \Phi_{dp}/2)} S''_{hh} + S''_{hv}) \tag{12}$$

$$V_v = CT_{vv}^2 (S''_{vv} + \xi e^{-j(\Phi_t + \Phi_{dp}/2)} S''_{hv}), \tag{13}$$

where

$$\xi = |T_{hh} / T_{vv}| = \exp(-\Gamma_h + \Gamma_v) . \tag{14}$$

The measured differential reflectivity can be expressed as

$$Z_{dr} = \frac{\overline{|V_h|^2}}{\overline{|V_v|^2}} = \xi^4 \frac{W_{hhhh} + \xi^{-2} W_{hvhv} + 2\xi^{-1} \mathrm{Re}\left(e^{j\Psi} W_{hhhv}\right)}{W_{vvvv} + \xi^2 W_{hvhv} + 2\xi \mathrm{Re}\left(e^{-j\Psi} W_{vvhv}\right)} \tag{15}$$

The measured differential phase is given by

$$\Phi_{DP} = \arg(\overline{V_h^* V_v}) = \Phi_{DP}^{sys} + \Phi_{dp} + \arg[W_{hhvv} + e^{-j2\Psi} W_{hvhv} + e^{-j\Psi}(\xi W_{hhhv} + \xi^{-1} W_{vvhv})] \tag{16}$$

In (15) – (16)

$$\begin{aligned} W_{hhhh} &= <|S''_{hh}|^2>, \quad W_{vvvv} = <|S''_{vv}|^2>, \\ W_{hvhv} &= <|S''_{hv}|^2>, \quad W_{hhvv} = <(S''_{hh})^* S''_{vv}>, \\ W_{hhhv} &= <(S''_{hh})^* S''_{hv}>, \quad W_{vvhv} = <(S''_{vv})^* S''_{hv}> \end{aligned} \tag{17}$$

$$\Phi_{DP}^{sys} = \Phi_t + \Phi_r , \quad \Psi = \Phi_t + \Phi_{dp}/2 \tag{18}$$

Overbars in (15) – (16) mean expected values and brackets in (17) stand for ensemble averaging.

The corresponding formulas for Z_{dr} and Φ_{DP} for alternate transmission / reception are obtained from (15) – (16) by setting the moments W_{hvhv}, W_{hhhv}, and W_{vvhv} to zero. It is important that, as opposed to the alternate scheme, the values of Z_{dr} and Φ_{DP} measured in the SHV mode depend on the system differential phase upon transmission Φ_t.

3 Model simulations

We perform our model simulations for a mixture of two snow species: polarimetrically isotropic snow aggregates and equioriented prolate crystals that produce depolarization. Concentrations and sizes of both species are assumed constant along the propagation path, whereas the canting angle of crystals is allowed to vary as shown in Fig. 3. The canting angle α is determined as the angle between the direction of the axis of rotation and the projection of the vertical onto the polarization plane.

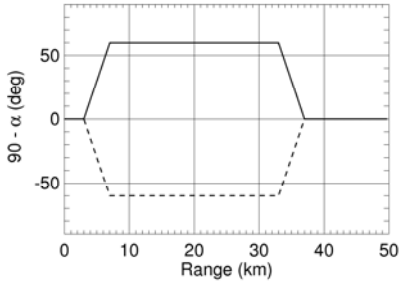

Fig.3. Two models of the canting angle varying with range.

The transmission matrix $\mathbf{T_{cr}}$ for nonuniform propagation path with varying canting angle α can be constructed as a product of transmission matrices related to small range bins (gates) within which propagation medium can be considered uniform

$$\mathbf{T_{cr}} = \prod_{n=1}^{N} \mathbf{T_n} \tag{19}$$

For each range bin Δr,

$$T_n = \begin{pmatrix} T_{hh}^{(n)} & T_{hv}^{(n)} \\ T_{vh}^{(n)} & T_{vv}^{(n)} \end{pmatrix} = \begin{pmatrix} d_b \cos^2\alpha_n + d_a \sin^2\alpha_n & (d_a - d_b)\sin\alpha_n \cos\alpha_n \\ (d_a - d_b)\sin\alpha_n \cos\alpha_n & d_b \sin^2\alpha_n + d_a \cos^2\alpha_n \end{pmatrix}, \tag{20}$$

where α_n is a canting angle in the n^{th} bin,

$$d_{a,b} = \exp(-j\gamma_{a,b}\Delta r) \quad , \tag{21}$$

and $\gamma_a - \gamma_b = K_{dp}$, where intrinsic specific differential phase K_{dp} depends on ice water content IWC and the shape of crystals but not on their canting angle.

Simulated radial profiles of Z_{DR} and Φ_{DP} for two models of the radial dependencies of the canting angle in Fig.3 are displayed in Fig. 4. In both cases, simulations were performed for three values of the phase $\Psi = \Phi_t + \Phi_{DP}/2$: 0, π/2, and –π/2. It was also assumed that IWC of crystals is equal to 0.5 g m^{-3}, intrinsic

Z_{DR} of crystals is 2 dB if they are oriented horizontally, and the radar reflectivity of crystals is 10 dB lower than the one from aggregated snow.

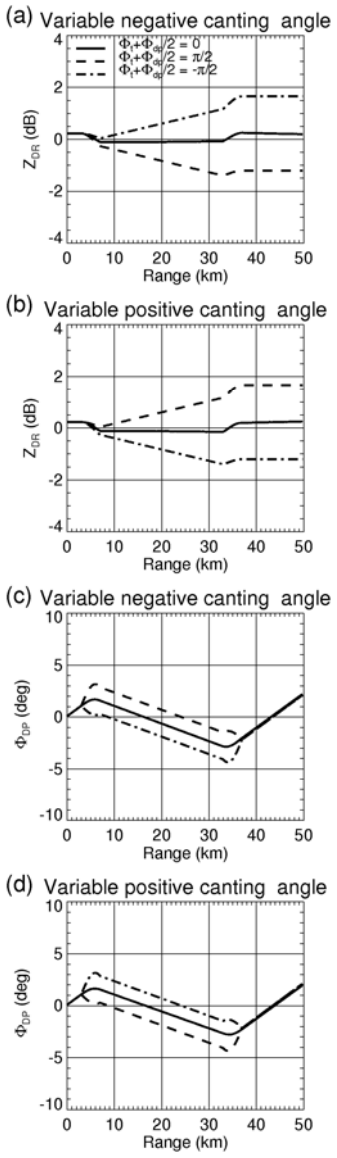

Fig. 4. Simulated radial profiles of Z_{DR} and Φ_{DP} in the cases of variable canting angle along the propagation path for different values of $\Psi = \Phi_t + \Phi_{dp}/2$ for simultaneous transmission / reception. The models of canting angle are illustrated in Fig. 3.

As Fig. 4 shows, depolarization effects due to canting cause substantial decrease or increase of Z_{DR} in the range interval where canting occurs (Fig. 4a,b). The sign and magnitude of this trend depends on the canting angle α and the phase Ψ.

Depolarization induces cross-polar components in the backscattered signal and gradually changes polarization state of the wave as it propagates through depolarizing medium. The latter effect, depolarization on propagation, explains the radial trend in Z_{DR} in the region of canted crystals although orientation of crystals and their shape is uniform there.

It is important, that at ranges beyond 37 km where crystals are not canted, the absolute value of Z_{DR} remains high compared to its "background value" of about 0.25 dB if $\Psi = \pm \pi/2$. This explains "radial streak" appearance of the Z_{DR} signatures in Fig. 1 and 2. Radial signatures of Z_{DR} are absent if polarization of incident wave is linear (45° slanted, $\Psi = 0$) or in the case of alternate transmission / reception.

The nonmonotonic range dependence of differential phase in Fig. 2 is also explained by the model. A slope of radial profile of Φ_{DP} in the region of canted crystals depends primarily on the canting angle: it is negative if $|\alpha| < \pi/4$ and positive if $|\alpha| > \pi/4$. In contrast, a slope of radial profile of Z_{DR} is determined by both canting angle and the phase Ψ. It is positive if $\alpha > 0$ and $\Psi > 0$ or $\alpha < 0$ and $\Psi < 0$. The slope is negative if $\alpha > 0$ and $\Psi < 0$ or $\alpha < 0$ and $\Psi > 0$.

4 Conclusions

Radial streaks in differential reflectivity Z_{DR} are commonly observed in the ice parts of thunderstorm clouds if a polarimetric radar simultaneously transmits and receives horizontally and vertically polarized waves (SHV mode of operation).

Such Z_{DR} signatures are not observed if the orthogonally polarized waves are alternately transmitted and received.

Radial Z_{DR} signatures in the SHV mode are attributed to cross-coupling between orthogonally polarized waves which is caused by depolarization in canted crystals that most likely acquire their orientation under the influence of strong electrostatic fields.

The impact of cross-coupling on Z_{DR} in the SHV mode depends on the system differential phase upon transmission Φ_t. It is minimal if $\Psi = \Phi_t + \Phi_{dp}/2 = 0$ and maximal if $\Psi = \pm \pi/2$. In the former case, polarization of incident wave is linear (45° slanted), whereas in the latter case it is circular. Z_{DR} measurements in the simultaneous and alternate transmission / reception modes are almost identical if $\Psi = 0$.

References

Doviak, R.J., V.N. Bringi, A.V. Ryzhkov, A. Zahrai, and D.S. Zrnic, 2000: Considerations for polarimetric upgrades to operational WSR-88D radars. *J. Atmos. Oceanic Technol.,* **17**, 257 – 278.

Ryzhkov, A.V., D.S. Zrnic, J.C. Hubbert, V.N. Bringi, J. Vivekanandan, E.A. Brandes, 2002: Polarimetric radar observations and interpretation of co-cross-polar correlation coefficients. *J. Atmos. Oceanic Technol.,* **19,** 340 - 354.